

Electrochemical Performance of $\text{LiFe}_x\text{Ni}_{0.5-x}\text{Mn}_{1.5}\text{O}_4$ Cathode Material for Lithium-Ion Batteries

Yakui Mu, Min Zeng*, Xin Wu, Xiaoling Tong

School of Materials Science and Engineering, Southwest University of Science and Technology, Mianyang 621010, P R China

*E-mail: zengmin@swust.edu.cn

Received: 22 March 2017 / Accepted: 29 April 2017 / Published: 12 June 2017

High-voltage anode material possess splendid application prospect in lithium ions battery. In this work, the Fe-doped $\text{LiFe}_x\text{Ni}_{0.5-x}\text{Mn}_{1.5}\text{O}_4$ ($x=0-0.5$) cathode materials have been synthesized by a solid-state method. The surface morphology and its composition have been characterized by X-ray diffraction, inductively coupled plasma, Field-emission scanning electron microscopy and Energy Dispersive Spectrometer. The physicochemical properties and electrochemical properties of the materials also have been investigated, and show that the as-prepared electrodes exhibit excellent cycling and rate performance than the $\text{LiNi}_{0.5}\text{Mn}_{1.5}\text{O}_4$ electrodes. It is considered that a little Fe^{3+} doping suppresses the generation of Mn^{3+} , and creates the charge vacancy, which can enhance the transportation of electron and lithium-ion in $\text{LiNi}_{0.5}\text{Mn}_{1.5}\text{O}_4$, which will guide the development of high-voltage cathode material in the future.

Keywords: Lithium-ion batteries; Fe-doped; additional lithium; cathode

1. INTRODUCTION

Due to the high energy density, long cycling life, low self-discharge, memory-free effect and environmental friendliness, Li-ion batteries (LIBs) are considered as one of the most promising large-scale energy storage systems used in EVs and HEVs [1-4]. To increase the performance of LIBs systems, cathode materials play an increasingly important role. However, all of the three established structural classes' cathode materials have some advantages and disadvantages: (i) Layered materials such as LiCoO_2 , $\text{Li}(\text{Ni}/\text{Co}/\text{Mn})\text{O}_2$ etc. mainly operating at about 4 V, have the advantages of high conductivity and suitable for high current charge/discharge, but also have the disadvantages of high cost and structural instability. (ii) Olivine materials such as LiFePO_4 (3 V), LiNiPO_4 , LiCoPO_4 (5 V materials) etc. has the advantages of high stability, safety, reliability, environmental protection and low

cost, but have the disadvantages of low theoretical capacity and low conductivity. (iii) Spinel materials such as LiMn_2O_4 (4 V material) has the advantages of low cost, high safety and easy preparation, but have the disadvantages of low theoretical capacity and structural instability [1-6].

To overcome these obstacles and meet the increasing requirements for large-scale energy storage, it is very significant to develop new high-performance cathode materials [1]. Recently, spinel $\text{LiNi}_{0.5}\text{Mn}_{1.5}\text{O}_4$ has received much attention due to the high operating voltage (4.7V vs Li/Li^+), low cost, environmental benignancy, lower toxicity and fast three-dimensional lithium-ion diffusion paths compared to the existing cathode materials [7-11]. Unfortunately, the Jahn-Teller distortion and the Mn^{3+} dissolution of $\text{LiNi}_{0.5}\text{Mn}_{1.5}\text{O}_4$ could result in rapid capacity decay and poor cycling performance [1, 10]. So far, a variety of strategies have been developed to overcome these drawbacks, ranging from cation doping [10-16] and synthesize a lithium additional materials [1] to approaches including nanosizing [17-19] and coating [20-24]. It was reported that partial cation substitution (Co [2, 6], Cr [6, 10, 12], Ru [13], Mg [14] and Al [16]) of Ni or Mn was found to be a highly promising approach, in increase the capacity, rate capability as well as capacity retention. Among these metal-doping, Fe is one of the most attractive candidates, due to its abundance, cost effectiveness as well as environmentally compatibility [12, 15, 21-23]. In this study, we utilized Fe^{3+} as a dopant not only due to its radius is approximate to Ni^{2+} and the three electrons in its 3d energy level which retains less Jahn-Teller distortion, but also Fe^{3+} diffuses into the $\text{LiNi}_{0.5}\text{Mn}_{1.5}\text{O}_4$ lattice and partially substitute for Ni^{2+} ions that could result in an increase of the hole concentration in $\text{LiNi}_{0.5}\text{Mn}_{1.5}\text{O}_4$ and thus enhancing the electrical conductivity. Electrochemical investigations indicate that our materials possess a high reversible capacity, excellent cycling performance and good rate capability.

2. EXPERIMENTAL

2.1. Synthesis of Fe-doped $\text{LiNi}_{0.5}\text{Mn}_{1.5}\text{O}_4$

$\text{LiFe}_x\text{Ni}_{0.5-x}\text{Mn}_{1.5}\text{O}_4$ ($x=0-0.5$) was synthesized by the traditional solid-state method [6]. In brief, Li_2CO_3 , NiO , MnO_2 and Fe_2O_3 were mixed according to the molar ratio and milled homogeneously in an agate mortar. And the homogeneous mixtures were calcined in air from 20°C to 850°C at a heating rate of 5°C min^{-1} and then kept at 800°C for 20h. Subsequently, the resultant product must be milled again to adjust the grain size of the coarse particles caused by high-temperature calcinations.

2.2. Materials Characterizations

The composition of prepared samples were tested by Inductively coupled plasma (ICP) analysis on 6500 analyzer (ThermoFisher). The structural and crystallographic analyses of the materials were characterized by X-ray diffraction (XRD) using an X-ray diffraction analyzer with $\text{Cu-K}\alpha$ radiation (X'Pert PRO, PANalytical) at the range of 10 to 80° .

2.3. Electrochemical Measurements

The working electrodes were fabricated by mixing 80 wt % active materials with 10 wt % super P and 10 wt % polyvinylidene fluoride (PVDF) dissolved in N-methyl-2-pyrrolidone (NMP). Then this uniform slurry was cast onto aluminum foil and then dried at 120 °C for 24 h. Subsequently, these electrodes were punched into disks and assembled into CR2016 coin half-cells in an Ar-filled glove box with Li foil as counter electrodes and polypropylene microporous film (Celgard 2300) as the separators [3, 6]. The commercial electrolyte was brought from CAPCHEM in China. Galvanostatic charge and discharge cycles were operated on a LAND battery test system at a current rate of C/10 (1C=147 mAh g⁻¹) between 3.5 and 5.0 V vs. Li/Li⁺ at room temperature.

3. RESULTS AND DISCUSSION

To determine the exact chemical compositions of Mn, Ni and Fe in the obtained LiFe_xNi_{0.5-x}Mn_{1.5}O₄ samples, ICP measurement was conducted. Table 1 indicates that the chemical compositions of these samples are consistent with the stoichiometric ratio as designed, and similar to the results in the literature. The XRD pattern of LiFe_xNi_{0.5-x}Mn_{1.5}O₄ (x=0-0.5) is shown in Fig. 1.

Table 1. Composition analysis data of the LiFe_xNi_{0.5-x}Mn_{1.5}O₄ samples by the ICP data.

	Material/element	Li	Mn	Ni	Fe
(a) x=0	LiNi _{0.5} Mn _{1.5} O ₄	0.98	1.49	0.5	—
(b) x=0.1	LiFe _{0.1} Ni _{0.4} Mn _{1.5} O ₄	0.98	1.49	0.39	0.11
(c) x=0.2	LiFe _{0.2} Ni _{0.3} Mn _{1.5} O ₄	0.99	1.5	0.3	0.21
(d) x=0.3	LiFe _{0.3} Ni _{0.2} Mn _{1.5} O ₄	0.99	1.5	0.19	0.31
(e) x=0.4	LiFe _{0.4} Ni _{0.1} Mn _{1.5} O ₄	0.98	1.49	0.1	0.42
(f) x=0.5	LiFe _{0.5} Mn _{1.5} O ₄	0.99	1.5	—	0.51

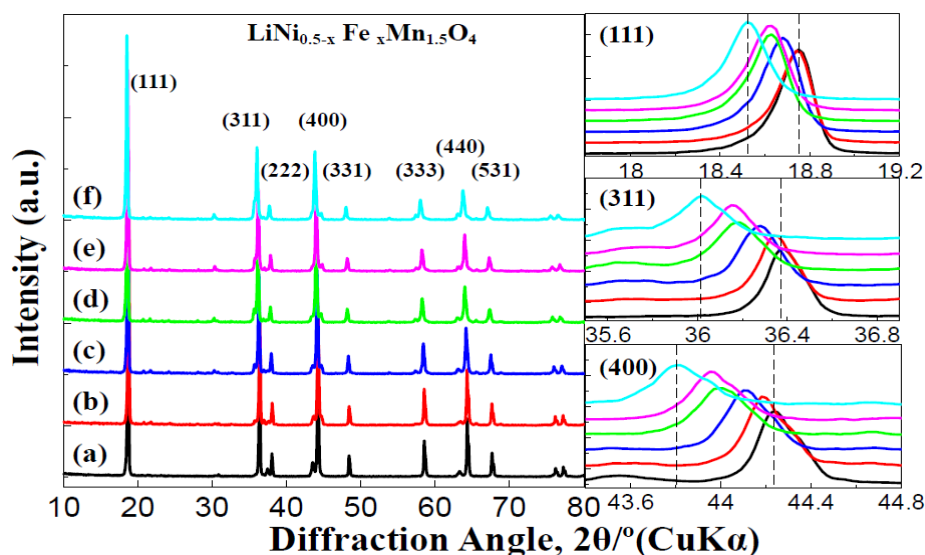


Figure 1. XRD patterns of LiFe_xNi_{0.5-x}Mn_{1.5}O₄, (a) x=0 (b) x=0.1 (c) x=0.2 (d) x=0.3 (e) x=0.4 (f) x=0.5.

The characteristic diffraction peaks of the samples correspond to the (111), (311), (400), and the other planes of well-crystallized cubic $\text{LiNi}_{0.5}\text{Mn}_{1.5}\text{O}_4$ (Fig.1(a), JCPDS No. 80-2162) and $\text{Li}_2\text{FeMn}_3\text{O}_8$ (Fig.1(f), JCPDS No. 48-0258), which fits well to the space group of $Fd\bar{3}m$, consistent with previously reported data [23, 24]. This result implies that the doping Fe^{3+} do not change the original $\text{LiNi}_{0.5}\text{Mn}_{1.5}\text{O}_4$ structure. However, very weak peaks at 37.5° and 43.5° are detected in the XRD results for the $x=0, 0.1$ and 0.2 samples, which could be attributed to the rock-salt phase impurities ($\text{Li}_y\text{Ni}_{1-y}\text{O}$, ICSD No.71422) originated from the oxygen loss in the samples at high annealing temperatures above 750°C [13]. On the other hand, very weak peaks at 30.3° and 35.7° for the $x=0.3, 0.4$ and 0.5 samples, which could be attributed to the residual reactive substance (Fe_2O_3 , ICSD No.39-1346), as shown in Fig. 1. Besides, the corresponding lattice constant was calculated according to the Scherrer formula. The results show, because the radius of Fe^{3+} (0.645 \AA) is larger than that of Ni^{3+} (0.61 \AA), [12, 21, 23] that the lattice constant (cubic, $a=b=c$) is increased from 8.178 \AA to 8.251 \AA for $\text{LiFe}_x\text{Ni}_{0.5-x}\text{Mn}_{1.5}\text{O}_4$ ($x=0-0.5$), respectively.

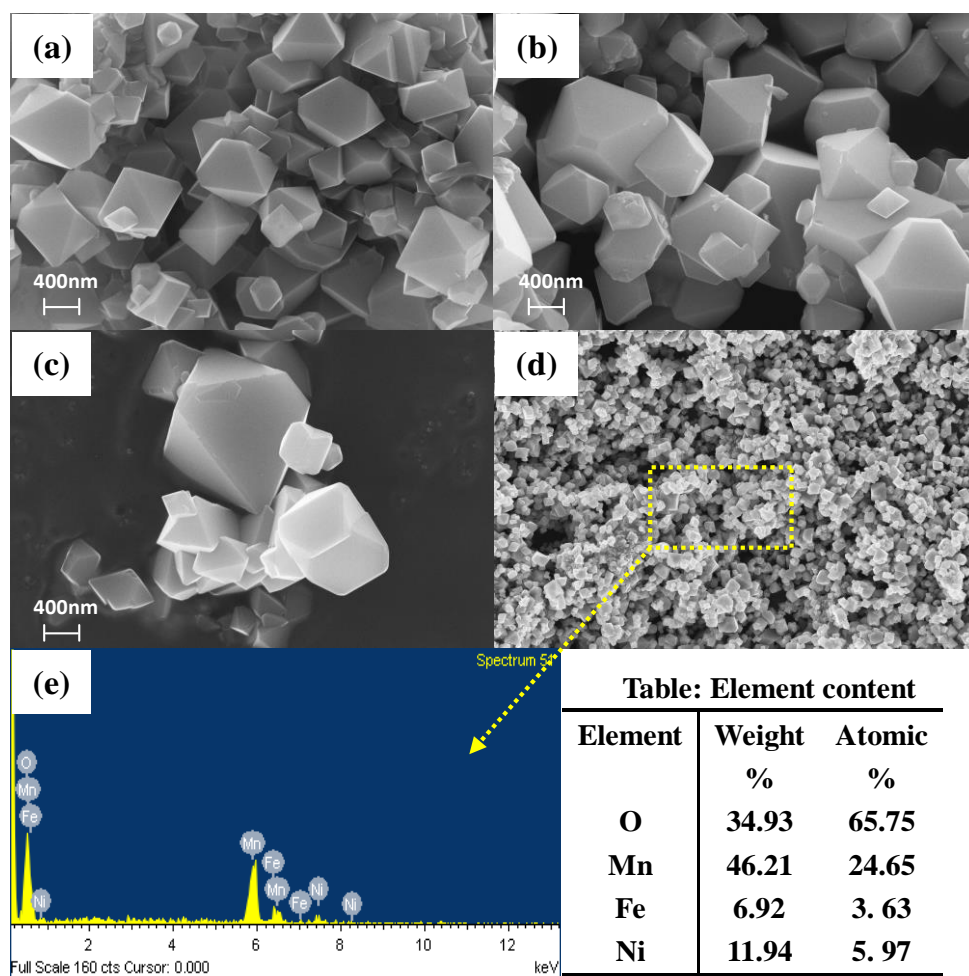


Figure 2. FESEM images of (a) $\text{LiNi}_{0.5}\text{Mn}_{1.5}\text{O}_4$, (b) (d) $\text{LiFe}_{0.2}\text{Ni}_{0.3}\text{Mn}_{1.5}\text{O}_4$ and (c) $\text{LiFe}_{0.5}\text{Mn}_{1.5}\text{O}_4$ samples, (e) SEM-EDS images and Element content of $\text{LiFe}_{0.2}\text{Ni}_{0.3}\text{Mn}_{1.5}\text{O}_4$ samples.

The morphology and structure of $\text{LiNi}_{0.5}\text{Mn}_{1.5}\text{O}_4$, $\text{LiFe}_{0.2}\text{Ni}_{0.3}\text{Mn}_{1.5}\text{O}_4$ and $\text{LiFe}_{0.5}\text{Mn}_{1.5}\text{O}_4$ were illustrated and shown in Fig. 2 (a-c), by field emission scanning electron microscopy (FESEM). It can be seen that the Fe-doped has a clear influence on the surface morphology and particle size, although the particles all exhibit a pseudo-octahedral shape. The pristine $\text{LiNi}_{0.5}\text{Mn}_{1.5}\text{O}_4$ sample has smooth surfaces and uniform particle size distribution about 200-300nm, as shown in Fig. 2 (a). However, the edges become less defined, the particle size also becomes uneven and surfaces turn to be less smooth with increasing amount of Fe in the sample, as shown in Fig. 2 (b, c). In addition, the SEM-EDS images and Element content of $\text{LiFe}_{0.2}\text{Ni}_{0.3}\text{Mn}_{1.5}\text{O}_4$ samples shown in Fig. 2 (d, e), the corresponding atomic weight and atom numbers are also shown in Table, indicates that the chemical compositions of $\text{LiFe}_{0.2}\text{Ni}_{0.3}\text{Mn}_{1.5}\text{O}_4$ samples are consistent with the stoichiometric ratio as designed.

To investigate the potential application of $\text{LiFe}_x\text{Ni}_{0.5-x}\text{Mn}_{1.5}\text{O}_4$ ($x=0-0.5$) as LIBs cathodes, galvanostatic measurements were carried out at a constant current density of 0.1C ($1\text{C} = 147\text{mAh g}^{-1}$) between 3.5 and 5.0 V (vs. Li/Li^+), as seen in Fig. 3.

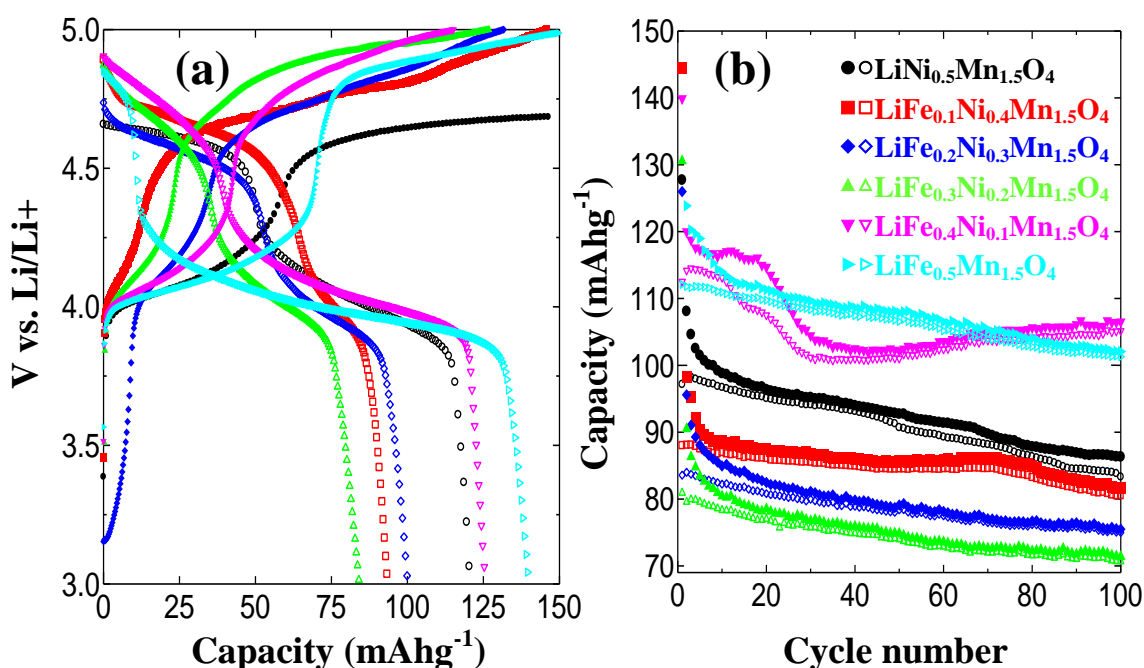


Figure 3. (a) The initial discharge/charge curves and (b) the cycling performance of the $\text{LiFe}_x\text{Ni}_{0.5-x}\text{Mn}_{1.5}\text{O}_4$ ($X=0-0.5$) samples.

The first charge/discharge process for all samples at 0.1C is shown in Fig. 3(a), a long voltage plateaus at 4.6–5.0V and this voltage increased with the Fe-doping increased can be observed. These experimental phenomena stem from that the $\text{Fe}^{3+}/\text{Fe}^{4+}$ redox voltage 5.0V is higher than that of the $\text{Ni}^{2+}/\text{Ni}^{4+}$ (4.7V), respectively. A small sloping plateau near 4.0 V also can be observed for all samples that stem from the $\text{Mn}^{3+}/\text{Mn}^{4+}$ redox couples [21, 23]. Experimental specific capacities (deinsertion, Q_D and insertion, Q_i) and coulombic efficiency ($Q_i/Q_D \times 100\%$) for the $\text{LiFe}_x\text{Ni}_{0.5-x}\text{Mn}_{1.5}\text{O}_4$ ($X=0-0.5$) samples was calculated from the discharge capacity of the first cycle (as shown in Fig. 2a), as displayed in Table 2.

Table 2. Experimental specific capacities (deinsertion, Q_D and insertion, Q_i), coulombic efficiency ($Q_i/Q_D \times 100\%$) of the first cycle, Q_i after 100 cycles and retention ratios for the $\text{LiFe}_x\text{Ni}_{0.5-x}\text{Mn}_{1.5}\text{O}_4$ ($X=0-0.5$) samples.

Sample	Q_D	Q_i	Q_i 3.5-4.1V	Q_i 4.1-5V	Coulombic efficiency	Q_i after 100 cycles	retention ratios
	(mAh g ⁻¹)	(%)	(mAh g ⁻¹)	(%)			
X=0	143.4	120.1	51.1	69	83.8	85.5	70.7
Refs[1]	121.9	-	16.5	-	-	-	92.5
Refs[8]	140	-	-	-	-	-	99.2
Refs[15]	121.4	-	14.9	-	-	-	-
X=0.1	143.5	93.2	24.3	68.9	64.9	82.7	87.9
Refs[6]	135	-	25.5	-	-	-	93.1
X=0.2	130.7	99.9	39.9	60	76.5	76.3	76.1
Refs[21]	137	-	-	-	-	-	93
X=0.3	126.7	83.6	35.4	48.2	65.9	73.5	87.3
X=0.4	134.9	113.1	59.0	54.1	83.8	105.4	92.8
X=0.5	141.6	121.2	87.0	34.2	85.6	102.9	84.2
Refs[23]	-	103	49	-	-	-	87.3

None of the samples reaches the theoretical capacity value of the $\text{LiNi}_{0.5}\text{Mn}_{1.5}\text{O}_4$ electrode (146.7mAh g⁻¹) or the $\text{LiFe}_{0.5}\text{Mn}_{1.5}\text{O}_4$ (148mAh g⁻¹), but similar to the results in the literature. By detailed analysis, we can observe, when $X < 0.3$, that the discharge capacity of Q_i at 3.5-4.1 V, which stem from the $\text{Mn}^{3+}/\text{Mn}^{4+}$ redox couples, decreased with the Fe-doping increased, and the capacity of Q_i at 4.1-5 V almost unchanged. The results show that the addition of Fe^{3+} can effectively inhibit the formation of Mn^{3+} . However, for the $\text{LiFe}_{0.4}\text{Ni}_{0.1}\text{Mn}_{1.5}\text{O}_4$ and $\text{LiFe}_{0.5}\text{Mn}_{1.5}\text{O}_4$ samples, may be due to the valence state of Fe^{3+} is higher than that of Ni^{2+} , the higher capacity of Q_i at 3.5-4.1 V clearly indicated that more Mn^{3+} is reduced.

The cycling performance of the samples at 0.1 C is shown in Fig. 3(b). The discharge capacities and the corresponding capacity retention ratios of the samples at room temperature retained after 100 cycles also been shown in Table 2. The reversible capacity of $\text{LiNi}_{0.5}\text{Mn}_{1.5}\text{O}_4$ is dramatically decreased after 100 cycles, whereas $\text{LiFe}_{0.1}\text{Ni}_{0.4}\text{Mn}_{1.5}\text{O}_4$ displays better cycling performance. It was clear that Fe^{3+} -doping can effectively inhibit the formation of Mn^{3+} and can improve the cycling stability, indicating that such long cycle performance of the ternary cathode material may be in large-scale application in the industry. The reversible capacity of $\text{LiFe}_{0.4}\text{Ni}_{0.1}\text{Mn}_{1.5}\text{O}_4$ is higher than the others, which may be attributed to the combined action of Fe^{3+} and Ni^{2+} , and which facilitate the diffusion of lithium ions and electrons.

The rate performance of the as-prepared samples was operated at various rates from 0.1 C to 1 C for ten cycles at each current density, as shown in Fig. 4. The 3rd cycles incremental capacity plots for room temperature annealed of the $\text{LiFe}_x\text{Ni}_{0.5-x}\text{Mn}_{1.5}\text{O}_4$ ($X=0-0.5$) samples with a cut-off current limit 0.1C between 3.5 and 5.0 V (vs. Li/Li⁺) were shown in Fig. 5. The change/discharge capacity of the $\text{LiFe}_x\text{Ni}_{0.5-x}\text{Mn}_{1.5}\text{O}_4$ ($X=0-0.5$) samples decreases at various rates from 0.1 C to 1 C, as shown in Fig. 4. This capacity fade is clearly related to the plateau at 4 V; therefore, it can be attributed to the Mn^{3+} dissolution in the electrolyte, as shown in Fig. 5.

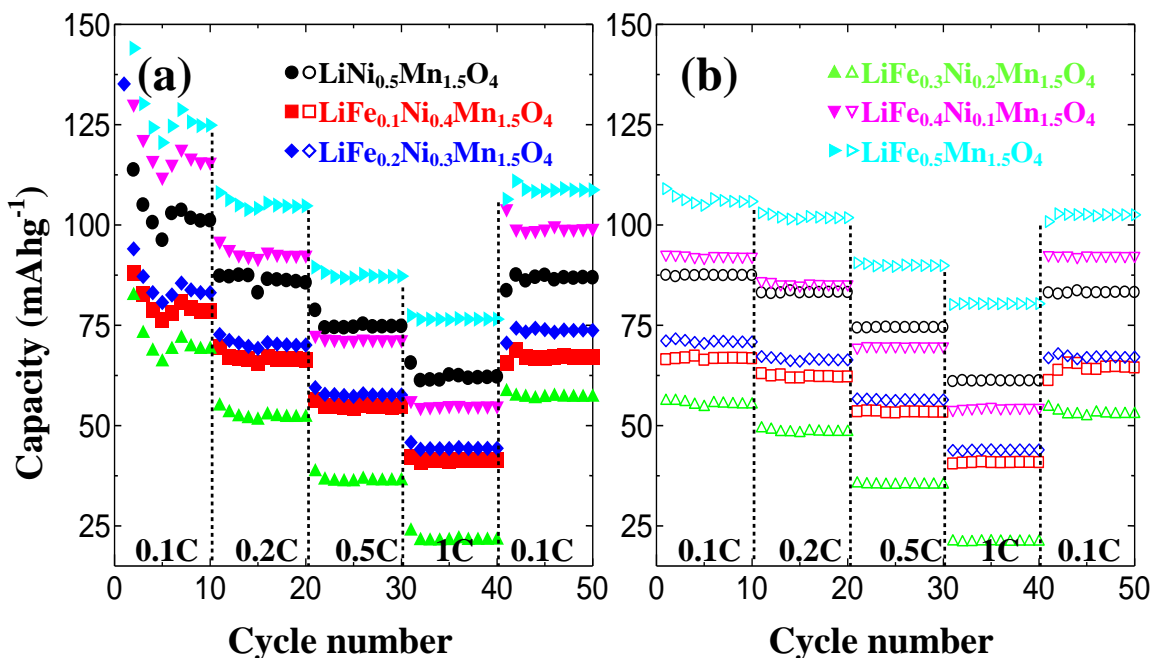


Figure 4. (a)The charge rate capability and (b) the discharge rate capability of the $\text{LiFe}_x\text{Ni}_{0.5-x}\text{Mn}_{1.5}\text{O}_4$ ($X=0-0.5$) samples.

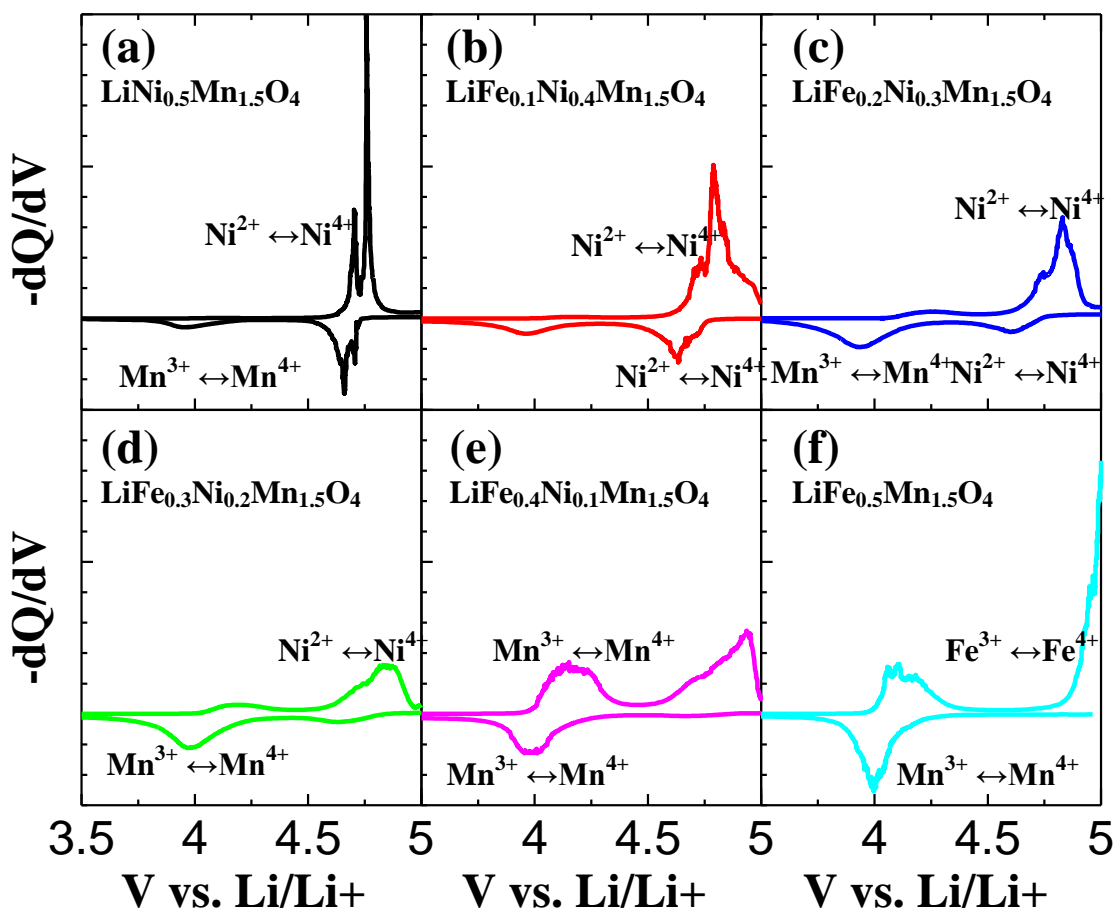


Figure 5. The 3rd cycle's incremental capacity plots for room temperature annealed of the $\text{LiFe}_x\text{Ni}_{0.5-x}\text{Mn}_{1.5}\text{O}_4$ samples: (a) $X=0$, (b) $X=0.1$, (c) $X=0.2$, (d) $X=0.3$, (e) $X=0.4$ and (f) $X=0.5$ with a cut-off current limit 0.1C between 3.5 and 5.0 V (vs. Li/Li^+).

Although the change/discharge capacity of $\text{LiFe}_{0.1}\text{Ni}_{0.4}\text{Mn}_{1.5}\text{O}_4$ and $\text{LiFe}_{0.2}\text{Ni}_{0.3}\text{Mn}_{1.5}\text{O}_4$ are smaller than that of $\text{LiNi}_{0.5}\text{Mn}_{1.5}\text{O}_4$, but the rate performances are better. These results demonstrate that Fe^{3+} plays a significant role on improving the rate capability of $\text{LiNi}_{0.5}\text{Mn}_{1.5}\text{O}_4$. These phenomena may be due to a little Fe^{3+} -doping that increases the charge vacancy and it can effectively inhibit the formation of Mn^{3+} , which we had discussed at before. On the other hand, the change/discharge capacity of $\text{LiFe}_{0.4}\text{Ni}_{0.1}\text{Mn}_{1.5}\text{O}_4$, that with the large amount of Fe^{3+} -doping, is higher than that of $\text{LiNi}_{0.5}\text{Mn}_{1.5}\text{O}_4$, but the rate performance is poor. It may be due to the stable structure and a little charge vacancy.

As shown in Fig. 5 (a), there are two main electrochemically active regions observed: at ~ 4.0 V and at ~ 4.7 V, which was corresponding to the $\text{Mn}^{4+}/\text{Mn}^{3+}$ and the $\text{Ni}^{4+}/\text{Ni}^{2+}$ redox couples, respectively [21-23]. The $\text{Ni}^{4+}/\text{Ni}^{2+}$ oxidation and reduction peaks become close to each other with increasing Fe^{3+} -doping, as shown in Fig. 5 (a-c), and the $\text{Mn}^{4+}/\text{Mn}^{3+}$ electrochemical activity is getting slightly more pronounced, which can be correlated to the amount of Mn^{3+} existing in the sample. Moreover, an additional peak in $\text{LiFe}_{0.5}\text{Mn}_{1.5}\text{O}_4$ is observed at around ~ 4.9 V in the oxidation step. This could be assigned to the $\text{Fe}^{4+}/\text{Fe}^{3+}$ redox couple and it increase with increasing Fe amount in the nominal composition, $\text{LiFe}_x\text{Ni}_{0.5-x}\text{Mn}_{1.5}\text{O}_4$, as shown in Fig. 5 (d-f). This also indicates that more Fe is doped into the spinel lattice with increasing 'x' value in $\text{LiFe}_x\text{Ni}_{0.5-x}\text{Mn}_{1.5}\text{O}_4$, even though the amount of the Fe_2O_3 impurity phase is increased [21, 23].

4. CONCLUSIONS

In summary, we synthesize modified $\text{LiFe}_x\text{Ni}_{0.5-x}\text{Mn}_{1.5}\text{O}_4$ ($x=0-0.5$) by a solid-state method as high-performance and high-voltage cathode materials for LIBs. There prepared electrodes exhibit excellent cycling and rate performance, which are much better than $\text{LiNi}_{0.5}\text{Mn}_{1.5}\text{O}_4$ electrodes. The superior electrochemical performance is ascribed to the Fe^{3+} , which creates the charge vacancy that can enhance the transportation of electron and lithium-ion in $\text{LiNi}_{0.5}\text{Mn}_{1.5}\text{O}_4$. Therefore, it is reasonable to conclude that the materials with Fe^{3+} doping and additional amount of lithium are very promising for use as cathodes in LIBs.

References

1. Y. X. Qian, Y. F. Deng, L. N. Wan and G. H. Chen, *J. Phys. Chem. C.*, 118 (2014) 15581.
2. J. Hassoun, K. S. Lee, Y. K. Sun and B. Scrosati, *J. Am. Chem. Soc.*, 133 (2011) 3139.
3. L. G. Wang, F. Y. Li and M. Zeng, *Int. J. Electrochem. Sci.*, 11 (2016) 9941.
4. H. Xu, M. Zeng, J. Li and X. L. Tong, *RSC Adv.*, 5 (2015) 91493.
5. H. W. Choi, S. J. Kim, Y. H. Rim and Y. S. Yang, *J. Phys. Chem. C.*, 119 (2015) 27192.
6. X. L. Tong, M. Zeng, J. Li, H. Xu, M. L. Du and F. Y. Li, *Int. J. Electrochem. Sci.*, 11 (2016) 7333.
7. N. Nitta, F. X. Wu, J. T. Lee and G. Yushin, *Mater. Today.*, 18 (2015) 252.
8. H. M. Cho, M. V. Chen, A. C. MacRae and Y. S. Meng, *ACS Appl. Mater. Inter.*, 7 (2015) 16231.
9. X. L. Zhang, F. Y. Cheng, J. G. Yang and J. Chen, *Nano Lett.*, 13 (2013) 2822.

10. D. Liu, W. Zhu, J. Trottier, C. Gagnon, F. Barray, A. Guerfi, A. Mauger, H. Groult, C. M. Julien, J. B. Goodenough and K. Zaghib, *RSC Adv.*, 4 (2014) 154.
11. C. Liu, Z. Y. Wang, C. S. Shi, E. Z. Liu and N. Q. Zhao, *ACS Appl. Mater. Inter.*, 6 (2014) 8363.
12. S. H. Oh, S. H. Jeon, W. Cho, C. S. Kim and B. W. Cho, *J. Alloy. Compd.*, 452 (2008) 389.
13. H. L. Wang, T. A. Tan, P. Yang, M. O. Lai and L. Lu, *J. Phys. Chem. C.*, 115 (2011) 6102.
14. M. H. Liu, H. T. Huang, C. M. Lin, J. M. Chen and S. C. Liao, *Electrochim. Acta.*, 120 (2014) 133.
15. J. Liu and A. Manthiram, *J. Phys. Chem. C.*, 113 (2009) 15073.
16. G. B. Zhong, Y. Y. Wang, X. J. Zhao and C. H. Chen, *J. Power Sources.*, 216 (2012) 368.
17. S. K. Hong, S. Mho, I. H. Yeo, Y. K. Kang and D. W. Kim, *Electrochim. Acta.*, 156 (2015) 29.
18. Z. X. Chen, S. Qiu, Y. L. Cao, X. P. Ai, K. Xie and H. X. Yang, *J. Mater. Chem.*, 22 (2012) 17768.
19. X. L. Zang, F. Y. Cheng, K. Zhang, Y. L. Liang, S. Q. Yang and J. Chen, *RSC Adv.*, 2 (2012) 5669.
20. J. W. Kim, D. H. Kim, D. Y. Oh, J. H. Kim and Y. S. Jung, *J. Power Sources.*, 274 (2015) 1254.
21. N. K. Yavuz, M. Yavuz, N. N. Bramnik and A. Bhaskar, *J. Power Sources.*, 327 (2016) 507.
22. D. L. Liu, Y. Bai, S. Zhao and W. F. Zhang, *J. Power Sources.*, 219 (2012) 333.
23. M. P. Pico, I. Á. Serrano, M. L. López and M. L. Veiga, *Dalton Trans.*, 43 (2014) 14787.
24. Y. Talyosef, B. Markovsky, R. Lavi, D. A. D. Kovacheva, E. Zhecheva and R. Stoyanova, *J. Electrochem. Soc.*, 154 (2007) 682-691.

© 2017 The Authors. Published by ESG (www.electrochemsci.org). This article is an open access article distributed under the terms and conditions of the Creative Commons Attribution license (<http://creativecommons.org/licenses/by/4.0/>).